https://doi.org/10.26565/2410-7360-2023-59-03
UDC 551.432.7+550.836+528.8+551.435.6

Received 25 September 2023
Accepted 27 October 2023

Evaluation of geological structures and geothermal resources in the North Tanzania Volcanic area using remote sensing and gravity data analysis

Albano Mahecha [1, 3]
Department of Corporative Program for Resources Engineering, Faculty of Engineering,
[1] Kyushu University, Fukuoka, Japan;
[3] Tanzania Geothermal Development Company Limited, Dar es Salaam, Tanzania,
e-mail: albanho6@gmail.com, https://orcid.org/0000-0001-9340-7448;
Nureddin Saadi [2]
Department of Geological Engineering, Faculty of Engineering, [2] University of Tripoli, Libya,
e-mail: n.saadi@uot.edu.ly, https://orcid.org/0000-0003-0593-8578;
Essam Aboud [4, 5]
Geohazards Research Center, [4] King Abdulaziz University, Jeddah, Saudi Arabia;
[5] National Research Institute of Astronomy and Geophysics, Cairo, Egypt,
e-mail: eaboudishish@kau.edu.sa, https://orcid.org/0000-0002-1087-1059;
Akira Imai [1]
Department of Earth Resources Engineering, Faculty of Engineering,
e-mail: imai@mine.kyushu-u.ac.jp, https://orcid.org/0000-0002-3058-9915;
Kotaro Yonezu [1]
Department of Earth Resources Engineering, Faculty of Engineering,
e-mail: yone@mine.kyushu-u.ac.jp, Scopus ID 22959316100

ABSTRACT

Problems Statement and Purpose. Northern Tanzania Volcanic terrain has been a subject of evaluation for geothermal potential in the last four decades. The region is characterized by Neogene to Recent volcanic and tectonic activities. This preliminary study based on remote sensing, water chemistry, gravity data, geological structures and volcanic centers distribution reports the geothermal manifestations identified and discusses the implications on geothermal fluid pathways. Oxygen-hydrogen isotope data from water samples indicate that there were involved in the hydrothermal system.

Tectono-Volcanic Structures. The Northern Tanzania Divergence (NTD) area characterized by Neogene to Recent volcanic and tectonic activities. Recent volcanic and tectonic activities are ash cone and lava dome eruption at the floor of Meru crater a century ago, dyke intrusion and volcanic eruption south of Gelai volcano, and Oldoinyo-Lengai volcano, respectively. Fumarolic activities and hot springs are dominant in a relatively young volcanic area to the north-eastern and northern part of the NTD.

Data and Methods. Shuttle Radar Topography Mission (SRTM), Landsat 8 Operational Land Imager (OLI) image, water isotope analysis and gravity data were used to extract and analyze the surface and subsurface geological lineaments and map the hydrothermal alteration zones in the study area. The hydrothermal alteration is used to evaluate and identify the permeable structures. Analysis and interpretation of the length and trends of extracted lineaments were used to investigate the tectonic evolution. Geological map of a study area was digitized from the existing geological maps and the age of rocks to delineate volcanic activity and associated lineaments based on the age of the lithological domain. Digital image processing was applied to enhance the visual interpretation. Gravity data were used to give insight into the subsurface structure in the study area.

Results and Discussion. The higher $\delta\ ^{18}O$ values and large deviation from meteoric water lines suggest that is due to the interaction of fluids with host rocks at elevated temperatures. These are consistent with open structures that act as conduits for fluid flow. The potential field gravity data reveal a basin-like structure trending in the NNW direction. The gravity data show that the basement units gradually deepen towards the central part and that it is controlled by two main fault systems that trend N-S and NW-SE respectively. The gravity data presented here provides new constraints on the tectonic evolution and geothermal resources of the study area.

Keywords*: Remote sensing, gravity, geothermal, Tanzania, Structures, Isotope.*

In cites: Mahecha Albano, Saadi Nureddin, Aboud Essam, Imai Akira, Yonezu Kotaro (2023). Evaluation of geological structures and geothermal resources in the North Tanzania Volcanic area using remote sensing and gravity data analysis. Visnyk of V. N. Karazin Kharkiv National University, series "Geology. Geography. Ecology", (59), 28-43. https://doi.org/10.26565/2410-7360-2023-59-03

1. Introduction

Located in the northern part of Tanzania, the study area is characterized by numerous hot springs, fumaroles and Neogene to recent volcanic and tectonic activities. The area presents the potential for geothermal resources and has been a subject of several volcanic and geothermal-oriented researches (Fairhead, 1980; Nzaro, 1970).

Remote sensing data with a combination of geophysical data has been applied over a number of applications in geoscience studies (Calvin et al., 2015). The applications range from mineral and geothermal exploration to volcanic activity monitoring. In geothermal exploration and volcanologic studies, remote

sensing data are widely used for mapping the geological structures, volcanic eruptive center distribution, thermal anomaly or surface temperature distribution, and hydrothermal alterations (Mia and Fujimitsu, 2013; Calvin et al., 2015; Ulusoy, 2016). On the other side, gravity data is widely used to study the geological structures and subsurface features in various geological and tectonic settings (Rymer and Brown, 1986; Simiyu and Keller, 1997).

In this study, Shuttle Radar Topography Mission (SRTM), satellite imagery data acquired from Operational Land Imager (OLI), water isotope analysis and gravity data are used to image surface and subsurface geological lineaments and map the hydrothermal alteration in the Northern Tanzania Volcanic area, with the aim of evaluating the geothermal resources and fluid pathways.

Three dominant structural trends (N-S, NW-SE and NE-SW) were recognized in the study area reflecting the tectonic setting of the Northern Tanzania Divergence (NTD). The gravity data show a deep graben structure in the central part of the study area. The different maxima of the horizontal gradient data indicate the existence of horst and graben blocks within the basin. The water isotopic analysis suggests that it has interacted with rocks at elevated temperatures before being discharged through permeable structures. The results provide constraints to the structure and tectonic history of the study area and an insight into the potential of future geothermal exploration in the North Tanzania Volcanic area.

2. Approach and Material

The hydrothermal alteration is used to evaluate and identify the permeable structures extracted from SRTM data (Mshiu et al., 2015). Statistical analysis of lineament length and trends based on the age of the geological formations provides useful information about the tectonic evolution of the area of interest (Saadi and Watanabe, 2008). Principal Component Analysis (PCA) and color normalization transformation (Chavez et al., 1991) were used to evaluate their efficiency in improving the visual interpretation and identifying the hydrothermal alterations in this study.

Gravity data provides a general overview of the subsurface structure in the area of interest (Bilim, 2007). A horizontal gradient (HG) filter is applied to the gravity data to locate the edges of the geological structure (Pilkington, 2007).

A total of nine (9) water samples from hot spring, surface and lake water were collected from the study area for isotope analysis to identify the origin of water and how water interacts in subsurface conditions.

3. Geological Setting

The Great Rift of East Africa is an approximately N-S trending structure extending from the Gulf of Aden, NE Africa to Mozambique, SE Africa (Fig. 1). It is comprised of two branches; the eastern arm which is referred as "Gregory Rift" and the western arm referred as "Albertine Rift". Gregory Rift extends from the Gulf of Eden through Ethiopia and Kenya to northern Tanzania where the Rift seems to be widening from approximately 50 km in southern Kenya to approximately 200 km wide splitting into three differently oriented branches; the Natron–Manyara, the Eyasi–Wembere and the Pangani rifts (Mollel et al., 2008). The NE - SW trending tilted fault blocks, south of Lake Natron, is referred to as Eyasi-Wembere Rift, NNE-SSW trending Manyara Rift and NNW - SSE trending Pangani fault system, south of roughly E-W volcanic chain of Essimingor – Kilimanjaro (Fig. 2); this split is referred as Northern Tanzania Divergence (Le Gall et al., 2008). The rift then continues to central Tanzania Archean Craton, at this point the rift is not as continuous as north of NTD. It extends further south to the triple junction intersecting with the Albertine Rift.

The structure of this elongated N-S rift is dominated by Ethiopian and Kenya domal uplift which geological studies and geochronological examinations have shown to have developed simultaneously with the rift system during Cenozoic faulting and volcanism (Fairhead, 1976).

The Neogene volcanic province of NTD is recognized to be younger than the volcanic provinces in Kenya and Ethiopia where magmatism commenced around 40 Ma (Baker et al., 1972; Dawson, 2008) suggesting mantle uprising is liable for intra-plate magmatism and crustal fracturing in this province (Dawson, 2008). The province is underlain by the Precambrian basement and bordered by Precambrian metamorphic rocks to the east and Archean craton rocks of central and northern Tanzania to the west. The province is dominated by Pliocene to recent volcanic and tectonic activities.

Previous geological studies confirmed that the major rift faulting episodes in northern Tanzania are around 2.1 Ma and 1.2 Ma (Wilkinson et al., 1986). It was also suggested that the existing rift escarpments progressed later than *c.* 1.2 Ma and major fault escarpments prevailed by *c.* 3 Ma (Foster et al., 1997).

Chronological studies indicated that the volcanoes of Essimingor, Oldoinyo Sambu, Ngorongoro, Monduli and Tarosero emerged between 4.8 - 2.01 Ma; then followed by the eruption of Ketumbeine, Gelai and Burko volcanoes (Fig. 5) and by effusion of trachy-basalt lavas between 1.5 - 0.6 Ma (Dawson, 2008; Mollel et al., 2008; Mana et al., 2015). The youngest volcanoes are Kerimasi, Kilimanjaro, Meru, and Oldoinyo Lengai which developed in 1 Ma (Wilkinson et al., 1986; Mana et al., 2015). The rock type of the volcanoes in the region is diverse varying

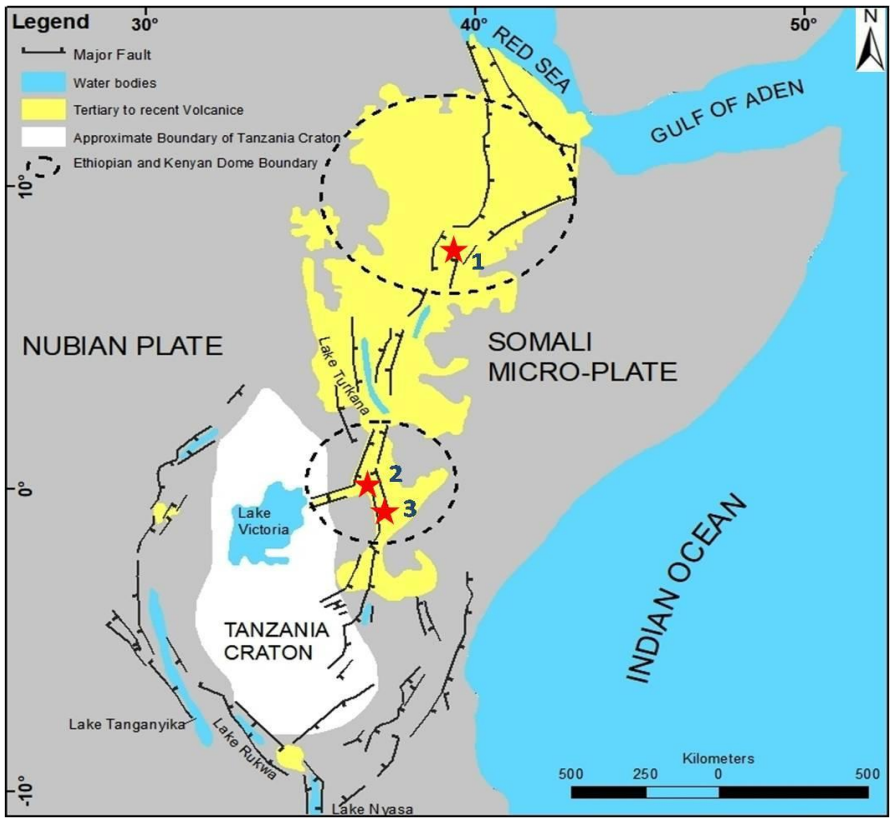

Fig. 1. Tectonic map of East Africa showing major faults, Tertiary to Recent volcanic and geothermal fields (after Dawson, 2008). Aluto Langano geothermal field with 8 MWe power plant (1), Menengai geothermal field (2) and Olkaria geothermal field (3), the largest geothermal field in Africa with installed capacity > 600 Mwe

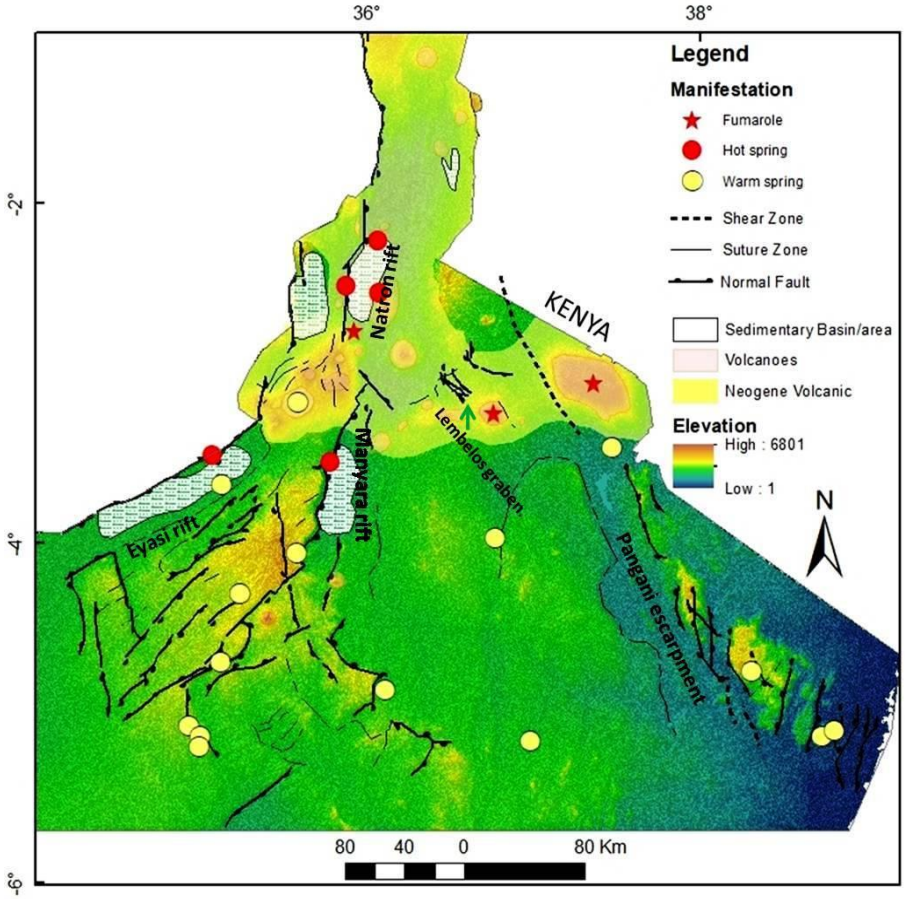

Fig. 2. The tectonic and general geology of Northern Tanzania.
Note the geothermal activities become more diffuse in the basement area south of the volcanic region, occurring in the form of warm springs (modified from Le Galle et al, 2008)

from basalt-trachyte-phonolite to nephelinite-phonolite associations (Fairhead, 1980; Dawson, 2008).

4. Data Processing

4.1 Remote sensing data

Satellite imagery and Digital Elevation Model (DEM) from the United States Geological Survey (USGS) are used in this work. The DEM derived from SRTM and Landsat imagery derived from OLI data (path 168/Row 062 and path 169/Row 062 acquired on October 13, 2016, and September 23, 2017, respectively). The spatial resolutions of the data sets are 3-arc seconds (approximately 90 m) and 30 m pixel resolution for SRTM and Landsat 8 respectively. These data sets are used to extract geologic lineaments, hydrothermal alterations and map the volcanic and tectonic landforms for the study area. The Landsat 8 band combinations were selected following initial experiments concerning the suitability of various band combinations to enhance the visual appearance and visual interpretation of geological lineaments (Saadi and Watanabe, 2008). The selected combinations have the advantage of preserving morphological features as well as displaying different lithological units in various colors because bands within the VNIR and SWIR portions of the electromagnetic spectrum were used (Sabins, 1997; Abdelsalam et al., 2000). Band 8 of Landsat 8 imagery (15 m) is used to enhance visual inspection of lineament extraction on SRTM data using Intensity-Hue-Saturation (IHS) Pan-sharpening (Mitchell, 2010).

Different azimuths of the sun are used to enhance and improve the image for visual interpretation. The sun angle used is 60º while sun azimuth varied from 45º to 315º to accommodate all possible trends of the lineaments under investigation.

Slope angle map of SRTM was used to recognize geological lineaments, volcanic centers, and cones in the study area (Fig. 3).

All lineaments and landforms observed within the shaded relief maps are manually mapped through on-screen digitization. The manual extraction criteria for lineaments and visual interpretation are based on image characteristics (tone and texture), lithological boundaries (rock units) and geomorphologic features (drainage patterns). Volcanic centers and their spatial distribution are mapped based on their circular shape and elevation above the immediate surrounding area specifically within the volcanic area. Hutchison et al. (2015) argued that the distribution and orientation of vents or craters can be used to assess the geometry of feeder dikes and eventually evaluate the structural controls on magma pathways.

The lineaments extracted from remote sensing data are aligned predominantly in the N-S direction, while the NW-SE and NE-SW trends are subordinate (Fig. 4). The extracted lineaments were divided into three groups based on age of the geological formations. Three formations were cut by the extracted lineaments; Precambrian, Plio-Early Pleistocene and Middle-Late Pleistocene (Fig. 5). Rose diagrams (Fig. 6) depict the distribution and orientations of lineaments on the three geological formations.

PCA (Fig. 7) and Directed Principle Component Analysis (DPCA) (Fig. 8) are applied to map the possible alteration patterns (Loughlin, 1991; Ali and Pour, 2014). DPCA (Pour et al., 2013) of four band ratios; 5/4 representing vegetation index, 4/2 for ferric iron oxide index, 6/5 for ferrous oxide index and 6/7 for hydroxyl/clay index (band ratio equivalent for OLI bands) has been applied to reduce the effects of vegetation in identifying the hydrothermal alterations. The principal component (PC) image combination of PC2:PC3:PC4 in RGB is used to discriminate different surface alterations, whereby PC2, PC3 and PC4 represent the transformation of band ratios of 4/2, 6/5 and 6/7 respectively. This allows detailed spectral characterization of surface targets, particularly of those belonging to the groups of minerals with diagnostic spectral features in this wavelength range. Pan sharpening of the resultant PC image was applied using band 8 of Landsat 8. Surface alteration is a result of fluid-rock interaction which indicates the fluid pathways, which can be used to map permeability. The importance of alterations is to identify the permeable zone on which hydrothermal fluid permeated to interact with the host rock.

4.2 Gravity data

The data was obtained from Sandwell and Smith (2009), and Sandwell et al., (2013, 2014) and used to delineate the possible subsurface structures in relation to the ones delineated from SRTM and satellite imagery (https://topex.ucsd.edu/cgi-bin/get_data.cgi). This data is corrected and ready to be used for interpretation and modelling (Sandwell and Smith (2009), Sandwell et al., 2013, 2014). Gravity map values range from -87 to 146 mGal (Fig. 9). The study area shows a basin-like structure, located in the central part of the area (blue anomalies). The volcanoes (pink anomalies) are located inside the basin and towards the edges. A profile was selected (AA') crossing the basin and some volcanoes to show the 2D structure (Fig. 10). Horizontal gradient analysis is used to enhance and sharpen the geological edges (Fig. 11). The horizontal gradient method has been used intensively to locate boundaries of density contrast from gravity or magnetic data (Ma et al., 2006; Bilim, 2007). It can be estimated from:

$$HG = \sqrt{Hx^2 + Hy^2} \qquad (1)$$

Where Hx and Hy are the derivatives in the x and y directions, respectively (Philips, et al., 2007).

Trends can be traced well, taking various directions (N-S, NE-SW, and E-W). The basin-like struc-

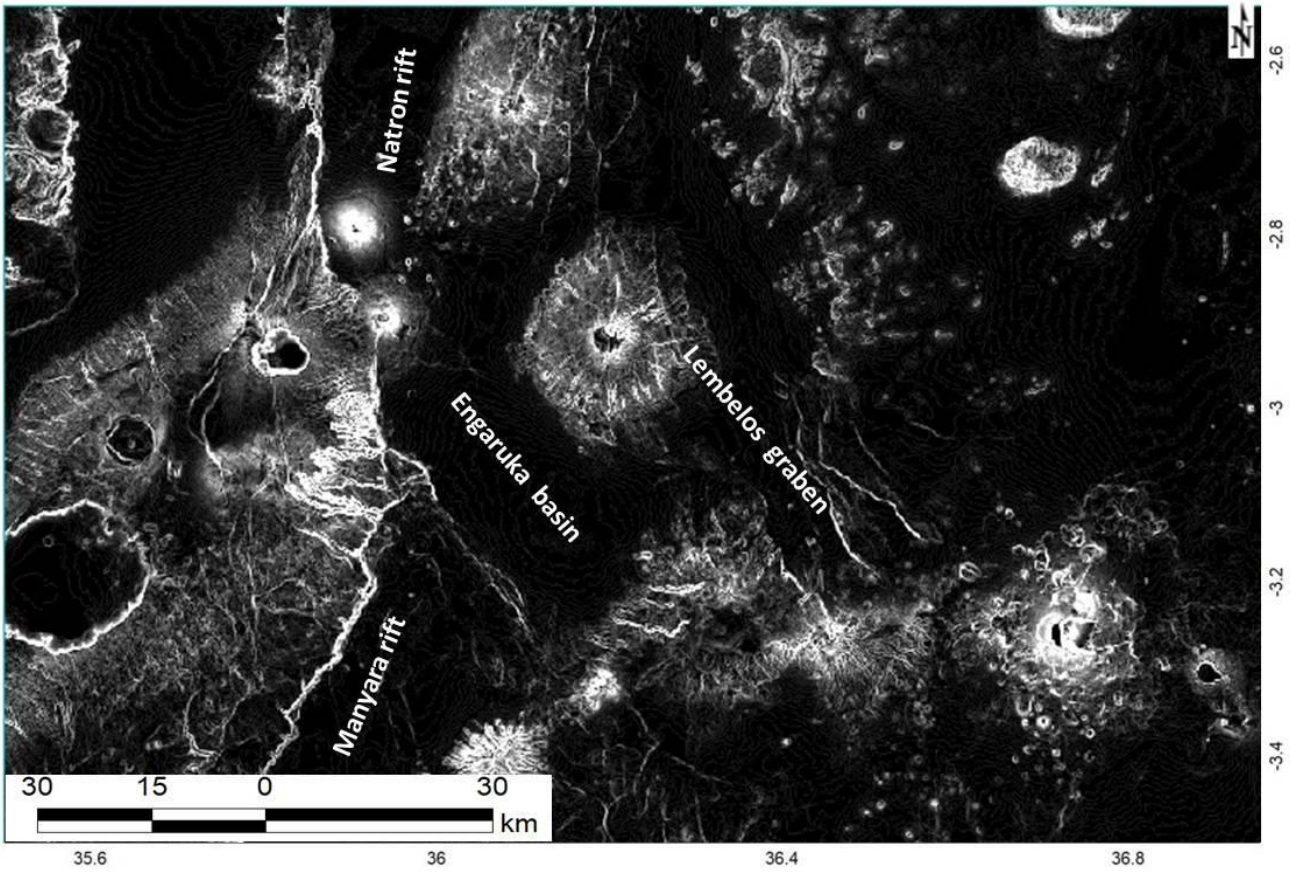

Fig. 3. Slope angle map of SRTM highlights geological lineaments (white line), volcanic centers, and cones (white spots) south East of Meru and South of Gelai Volcano

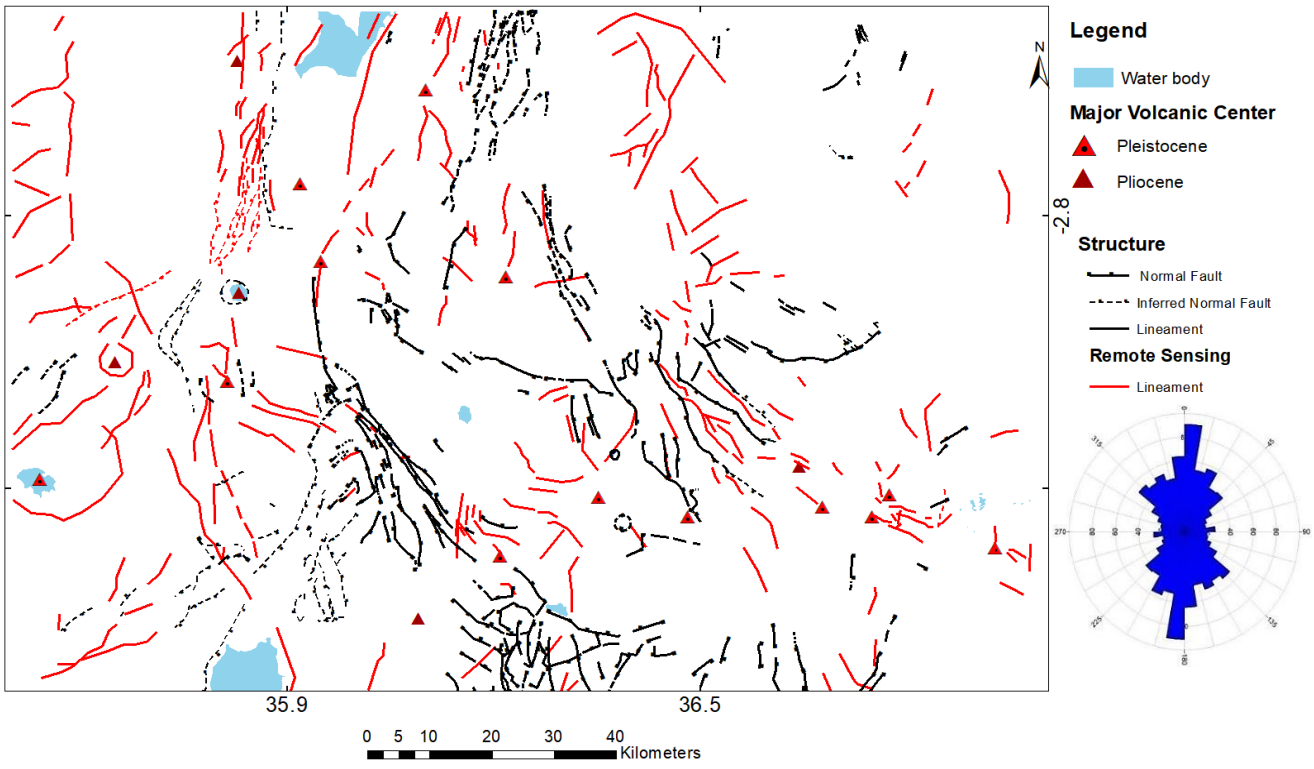

Fig. 4. Structural map of the study area, red color lineaments extracted from remote sensing data. The rose diagram shows the dominance of three major trends; N-S, NW-SE, and NE-SW. The N-S trend reflecting the East Africa Rift System general trend has a higher frequency, the rose diagram is based on azimuth frequency

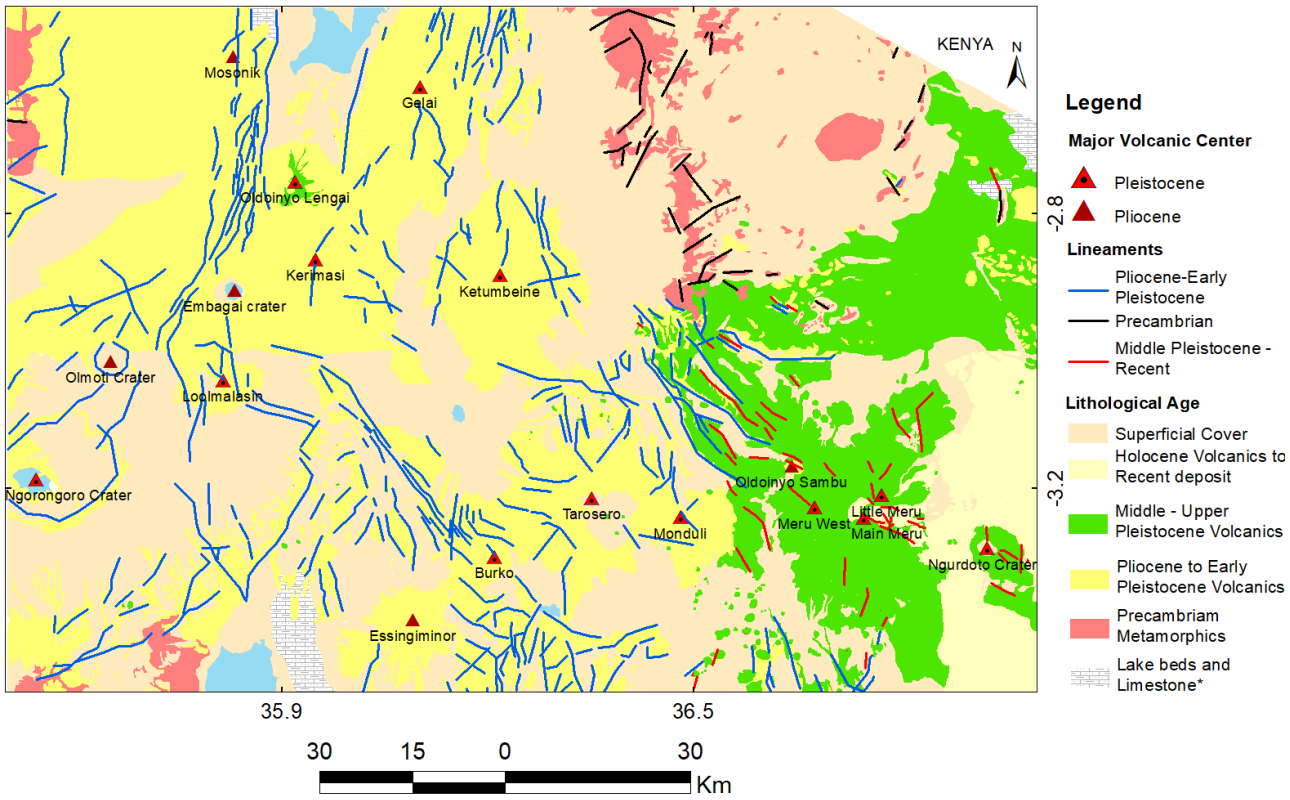

Fig. 5. Geology map of the study area based on age. Lineaments were overlaid on the map to deduce their association with the lithological age (*Age is unknown)

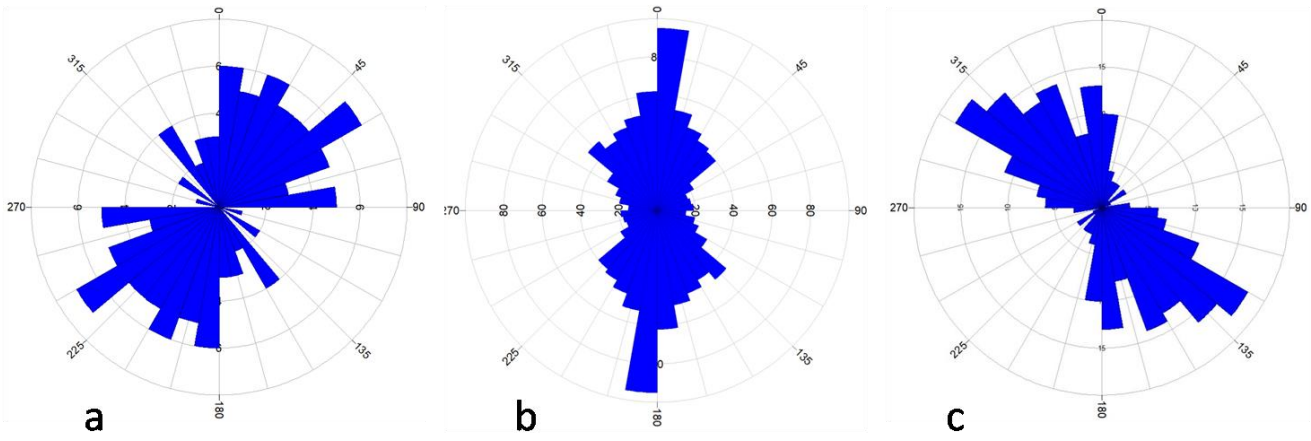

Fig. 6. The rose diagrams of the extracted lineaments based on the underlying age of the lithological domain. (a) Precambrian lineaments domain show the NE-SW trend which is considered to be pre-rift deformation, (b) represents the Plio-Early Pleistocene age which is predominantly N-S, during early magmatism and rifting episodes in northern Tanzania, and (c) Middle- Late Pleistocene age is dominated by the NW-SE structural trend and represents youngest volcanic and tectonic activity

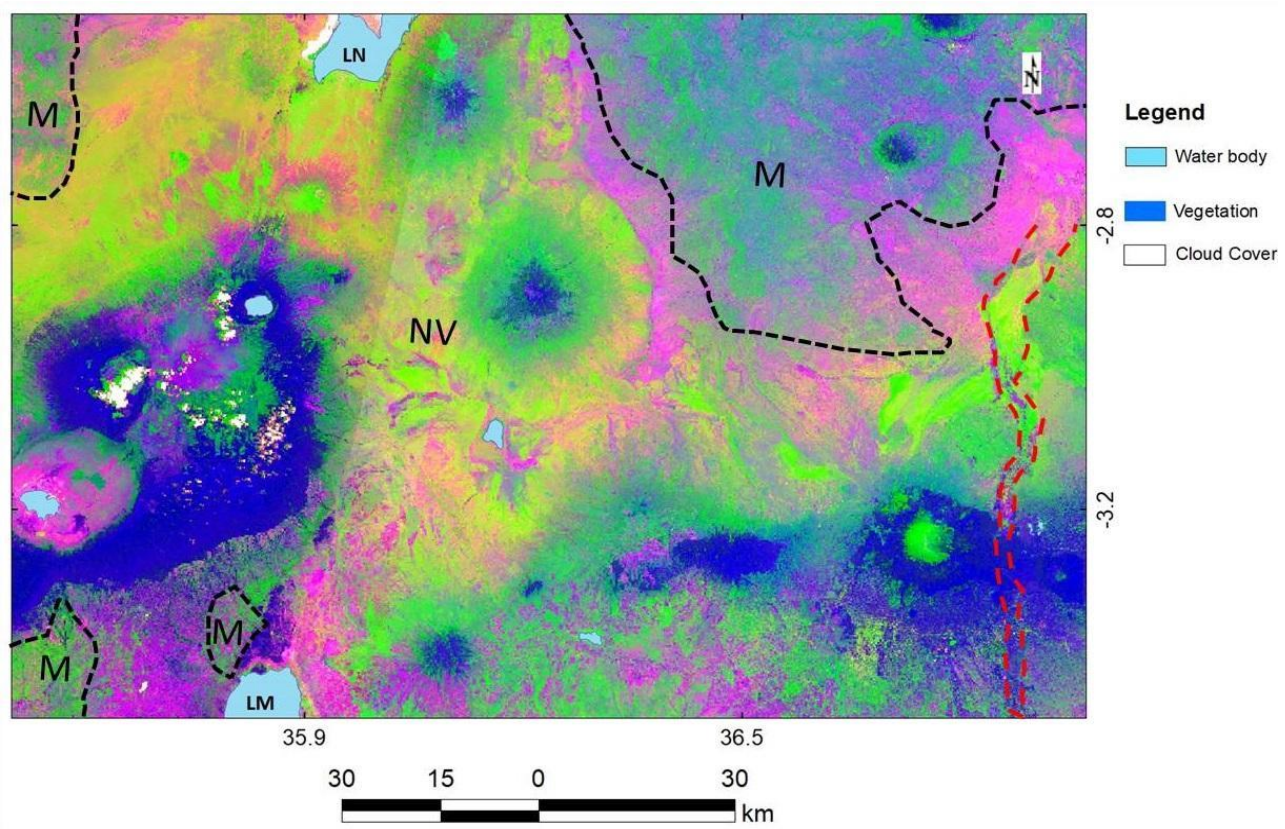

Fig. 7. Principal Component Analysis of six bands (2-7) image in RGB (PC1:PC2:PC3), used to mark the proximate boundaries of a dominant lithological domain in black color line and graben structure running N-S (red color) which is reflected on the low gravity anomaly of the section A-A'. The red color may represent the lake beds and limestone found in the respective areas. M= Precambrian Metamorphic; NV=Neogene Volcanic; LN=Lake Natron; LM= Lake Manyara

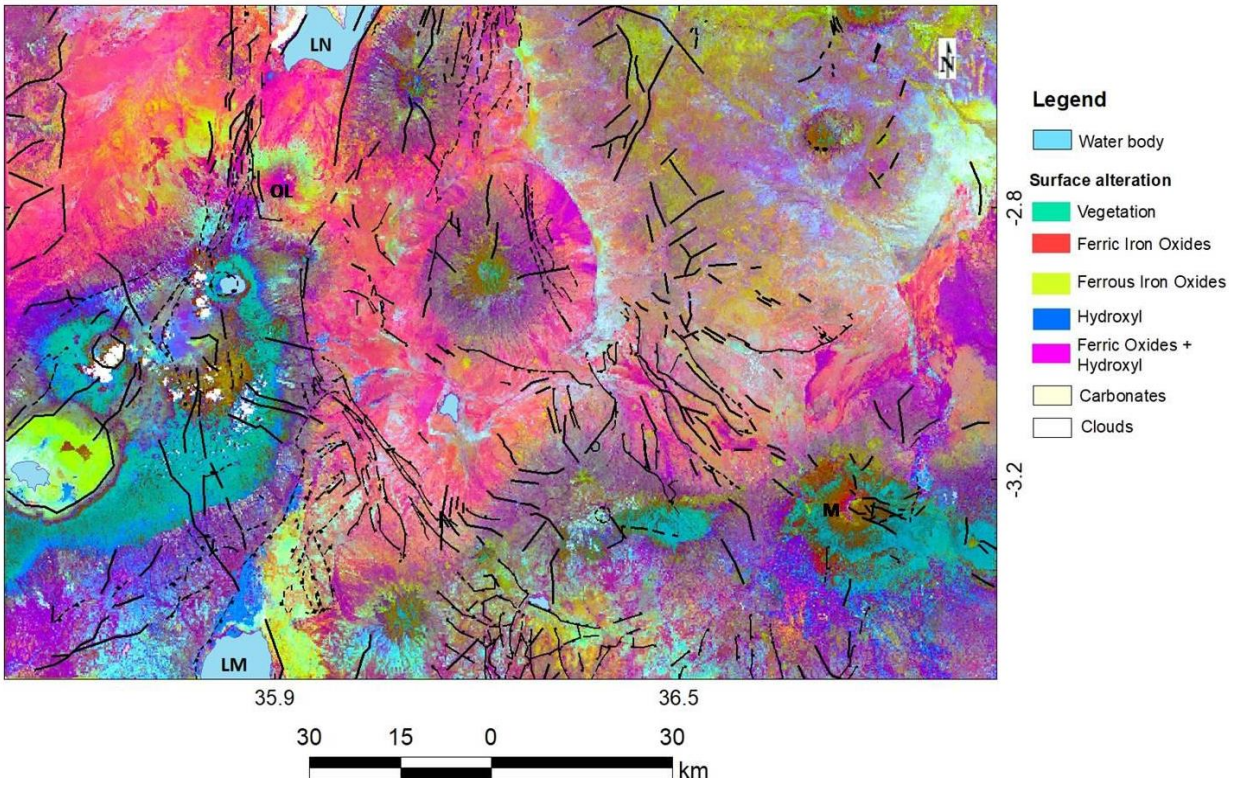

Fig. 8. Directional Principal Component Analysis (DPCA) of four band ratios (5/4, 4/2, 6/5, 6/7) are represented as RGB (PC2:PC3:PC4) overlaid by geologic structures. Ferric oxides dominate the volcanic area probably due to weathering of iron-bearing minerals in mafic volcanic rocks

ture extracted from the gravity map (Fig. 11) trending in NNW-SSE direction in the northern part and NE-SW in the southern part is well-matched with the SRTM slope angle map (Fig. 3). Notably, some anomalies have a circular shape and others have elongated shapes which indicate various structural features in the study area.

To get a more quantitative representation of the subsurface structure of the study area, a 2D gravity model was constructed along the NW-SE profile. The gravity model along the profile AA' is about 176 km long. The Analytic Signal (AS) method was used to calculate the depth to the basement on profile. This method is designed to be applied to magnetic data. When using gravity data, the vertical derivative of gravity is applied (Phillips, 1997; Nabighian, 1972, 1974). The basement is estimated at a depth of about 4 km in the central part to about 2 km east and west. This reflects the basement relief underneath the volcanic area.

4.3 Water Chemistry

Oxygen and hydrogen stable isotopic composition are used to identify the origin of the water. A total of nine (9) water samples from the study area and two (2) samples from the Olkaria geothermal field (Table 1). The fieldwork was conducted between 7th and 13th September 2017. Samples were analyzed using Liquid Water Isotope Analyzer (IWA-35/45EP) in Kyushu University Lab. SMOW (Standard Meteoric Ocean Water) and 11 water samples were set and measured 24 times for each. As the principal, this analyzer emits the laser to the samples and then, the isotopic composition is determined by comparing the intensity of the laser passing through samples and the original intensity of the laser. In the process of removing largely deviated data as outliers, Smirnov-Grubbs verification was applied. This verification assumes that the results measured 24 times for each sample are distributed normally. The results with low significance levels were removed. The first step of this verification is to calculate a formula (1).

$$|x\text{-ave}|/dev \qquad (2)$$

x (‰): most deviated δ value from average in 24 values;

ave (‰): average value of 24 values;

dev: standard deviation of 24 values.

If the result of equation (2) is more than Smirnov-Grubbs constant, x should be removed. After removing the value, the average and deviation have to be recalculated, and the same process will be perfumed in 23 samples. When the value of equation

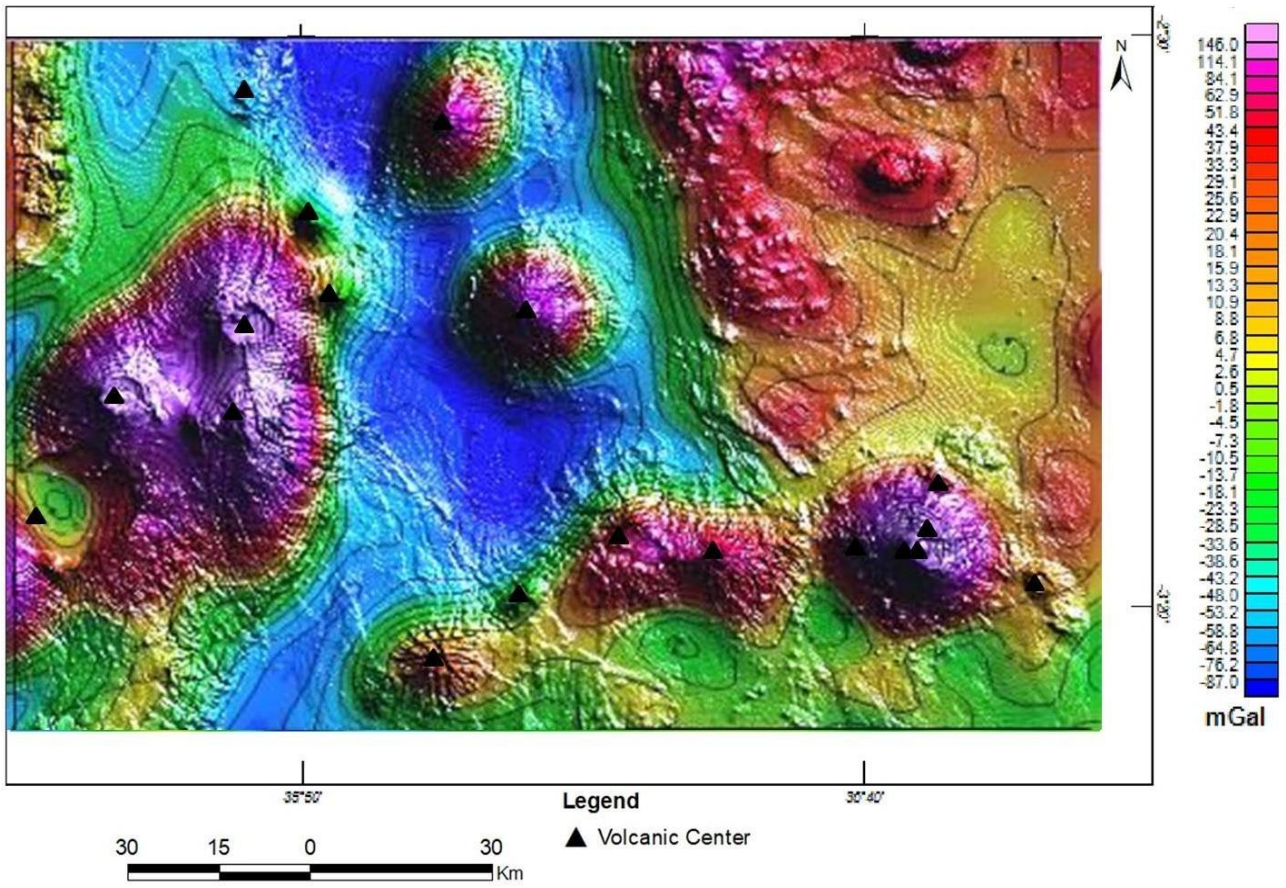

Fig. 9. Bouguer gravity map for the study area, high positive anomaly highlighted the volcanic features and low negative anomaly reflects a major structural trend N-S orientation. Volcanic features seem to be rooted in this major structural trend in a roughly N-S direction. Data source (https://topex.ucsd.edu/cgi-bin/get_data.cgi)

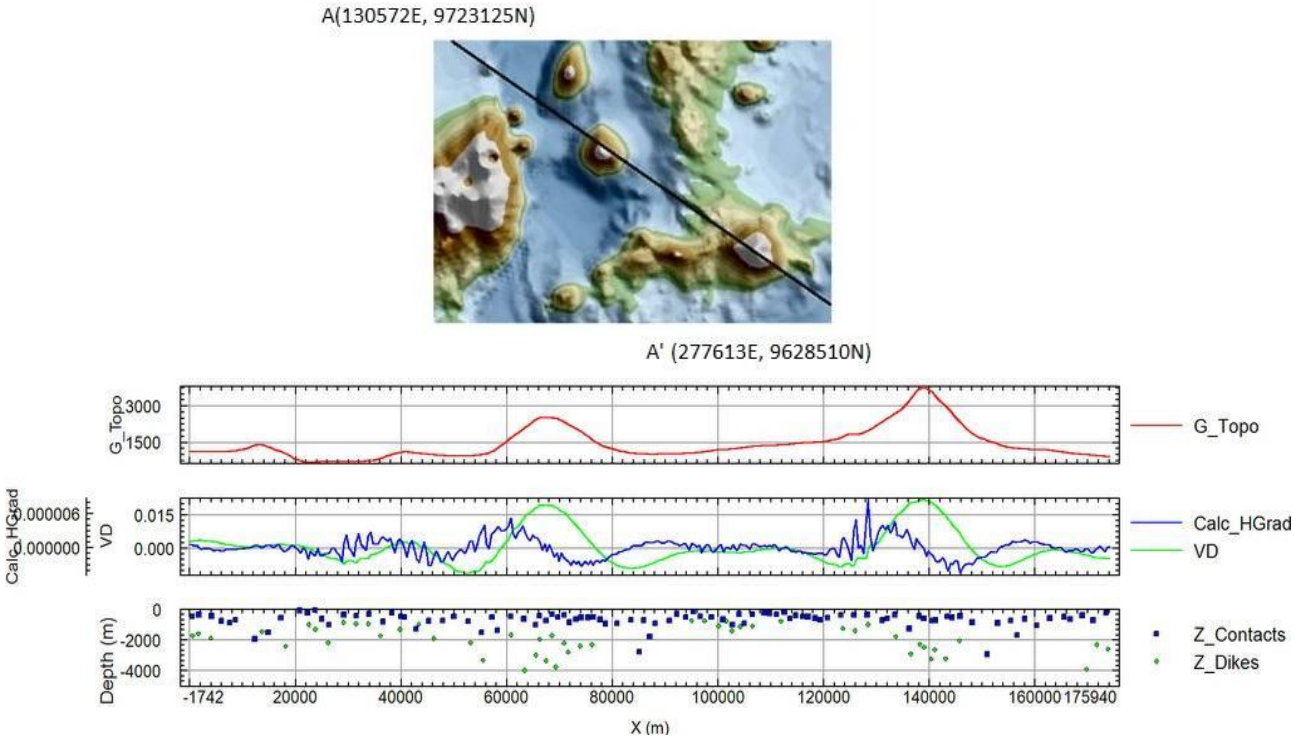

Fig. 10. Estimated depth to the basement using analytic signal method along the section AA'. The concentration of dikes is related to volcanoes across the section

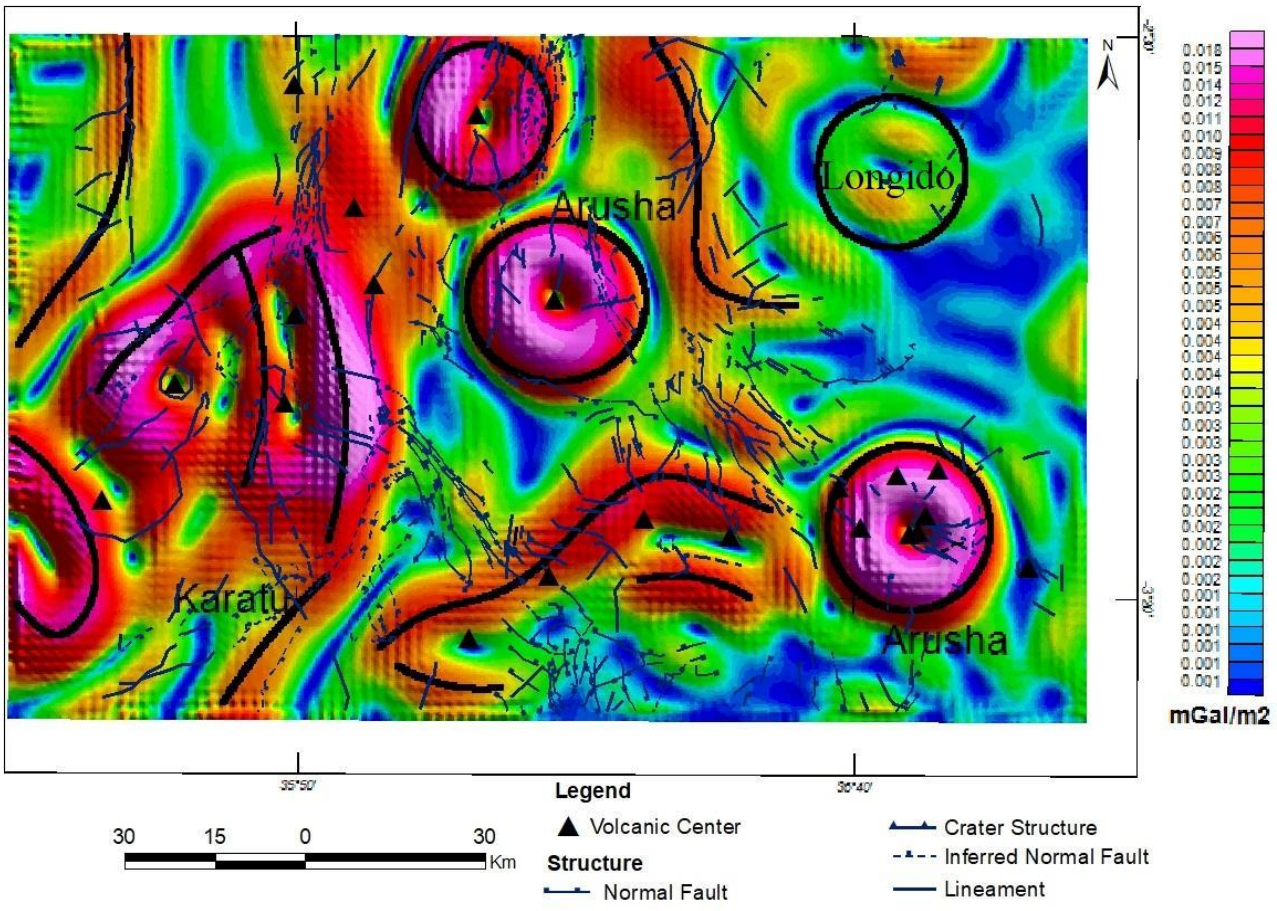

Fig. 11. Horizontal gradient map deduced from gravity data overlaid by geological lineaments extracted from remote sensing. Circles show borders of volcanic fields and thick black lines show the predicted structures. The circle on the top right corner is a Longido mountain, the circular shape and sharpness, suggest that it may be formed as a result of the magmatic intrusion

(2) is less than Smirnov-Grubbs's constant, then the result is regarded as liable. δD and δ ^{18}O values were calculated using the formulae (3) and (4):

$$\delta D\ (‰) = [(D/H)\ sample/(D/H)\ SMOW\text{-}1]/\times 1000 \quad (3)$$

$$\delta^{18}O\ (‰) = [(^{18}O/\ ^{16}O)\ sample/ (^{18}O/\ ^{16}O)\ SMOW\text{-}1] \times 1000 \quad (4)$$

A number of selected volcano-related geothermal fields and the onset age of magmatism which contributed to the geothermal system development are hereby revisited.

5. Discussion

NTD is a tectono-volcanic area characterized by Neogene to Recent volcanic and tectonic activities. Recent volcanic and tectonic activities are ash cone and lava dome eruption at the floor of Meru crater a century ago (Wilkinson et al., 1986), dyke intrusion and volcanic eruption south of Gelai volcano, and Oldoinyo-Lengai volcano, respectively (Albaric et al., 2010; Himematsu and Furuya, 2015). Fumarolic activities and hot springs are dominant in a relatively young volcanic area to the north-eastern and northern part (Kilimanjaro, Meru and Oldoinyo-Lengai) of the NTD. The regional geology map of a study area (Fig. 5) was digitized from the existing geological maps and the age of rocks (Wilkinson et al., 1986; Dawson, 1992; Mana et al., 2015) to delineate volcanic activity and associated lineaments based on the age of the lithological domain. Three dominant structural trends

Table 1

Water samples information

ID	Location	Type	Altitude (m)	pH	Temperature
Aru-G1	Meru Area	Groundwater	1448	9.65	23.9
Aru-L2	Meru Area (Small Momella)	Lake water	1444	9.68	22.8
Aru-L3	Meru Area (Tulusia)	Lake water	1441	10.1	25.8
Nat-H1	Lake Natron	Hot spring	602	9.76	48.3
Nat-H2	Lake Natron	Hot spring	602	9.77	50.8
Nat-H3	Lake Natron	Hot spring	601	9.77	50.1
Nat-H4	Lake Natron	Hot spring	605	9.77	45.6
Nat-H5	Lake Natron	Hot spring	608	9.75	49.7
Nat-H6	Lake Natron	Warm spring	605	9.74	31.7
Olk-H1	Olkaria area	Thermal water	2065	12*	71.7
Olk-H2	Olkaria area	Thermal water	2065	11*	79.5

*refers to quick measurement.

in the study area which reflect the tectonic setting of the NTD are identified, N-S, NW-SE and NE-SW (Fig. 4). Based on lithological domains; the NE –SW trending geological lineaments are dominant on the Precambrian rocks. The N-S and NW-SE structures are dominant and associated with Plio-Early Pleistocene and Middle-Late Pleistocene lithological domains, respectively. Mana et al. (2015) suggested that the Natron and Manyara Rift basin structures show north to south younging direction. On the other hand, early magmatism started in the southwestern area of the NTD and progressed towards the northern and eastern parts of the NTD.

Comparing NTD with other existing volcanic hosted geothermal fields, Rosenberg (2017) suggested that magmatism beneath the Wairakei geothermal field might have reinforced the development of a geothermal system during the past 0.3 Ma. At the Hengill-Hellisheidi geothermal field, the high-temperature geothermal system is associated with an age limit of about 0.4 Ma (Franzson et al., 2005).

Furthermore, more than 200 volcanoes extending SW-NE in the active tectono-volcanic zone of Iceland aged (< 0.8 Ma) host high-temperature geothermal fields (Björnsson, 2010). The volcanic activity at Menengai caldera, which hosts the geothermal field, is suggested to have started at 0.18 Ma (Leat, 1991). Very young volcanoes may not have the potential for sustainable geothermal resources due to the immaturity of a cap and possible heat exchange system which may support the heat storage.

Kerimasi, Gelai, Kilimanjaro, Meru, and Oldoinyo-Lengai volcanoes have been developed during the last ~1 Ma (Wilkinson et al., 1986; Mana et al., 2015). While Kerimasi, Gelai and Oldoinyo-Lengai volcanoes are accommodated in the N-S structural corridor, Meru volcano lies in the approximate location of intersection between the NW- SE and N-S structures, delineated from remote sensing, and the E-W structure delineated, from the gravity data (Fig. 9 and Fig. 11).

Ebinger et al. (2017) noted that pressurized magma chambers exist beneath Natron – Manyara zones, such as Oldoinyo-Lengai, Naibor Saito mono-

genetic cones complex, south of Gelai volcano and sill complex between Gelai volcano and Oldoinyo-Lengai. Furthermore, they argued that zones of seismicity beneath the Naibor Saito monogenetic cones may be a reflection of the presence of sills or to have been produced by hot, gas-rich magmatic fluids from the lower magma chamber. This is still an active system which continues to replenish this ~1Ma volcanic complex.

Lineaments deduced from gravity data highlight the existence of an E-W interesting 'hidden structure' (Essimingor – Meru volcanic chain). The trend of the NW-SE structures north of the volcanic chain could explain the onset of the development of 'transform fault' (Fairhead, 1980). South of roughly E-W trending volcanic chains of Essimingor – Meru chain, the geothermal and volcanic activity becomes more diffused. However, the Manyara Rift segment, on the western border fault, along the shore of the lake, which runs from the Magadi-Natron basin, hosts the hottest hot spring in the region about 70.8º C. It emanates from the basement rocks (Nzaro, 1970).

Slope modelling of SRTM data highlights major faults, major volcanoes and substantial presumed scoria/parasitic cones southeast of Meru volcano and the Naibor-saito monogenetic cone complex that is located south of Gelai volcano (Ebinger et al., 2017). Craters and calderas are well demarcated on the slope angle map (Fig. 3).

The dominant trend delineated from remote sensing is in line with the dominant low gravity anomaly running N-S, which has been interpreted as a subsurface structure and continuation of the East Africa Rift (Fig. 9). The horizontal gradient map (Fig. 11) shows the persistence of N-S structures and the roughly E-W subordinate structures associated with the extracted lineaments.

The gravity cross section running NW-SE (Fig. 10) depicts the low negative anomaly bodies in the lake Natron which may represent a deep structure possibly buried graben and probably altered zone with surficial alteration depicted on Landsat image (Fig. 8). The high positive anomaly coincides with Ketumbeine and Meru volcano and likely represents magmatic bodies. The low anomaly east of Meru volcano may represent a graben or an altered zone depicted on lineament extraction and PCA, RGB map of PC1, PC2 and PC3 (Fig. 7). Fairhead (1980) estimated the depth of volcanic and sedimentary pile to be 800 m at the Lembelos Graben NW of Meru, and depth to the basement to be around 1 km.

Patches of alteration deduced from the Landsat image display a dominant N-S orientation (Fig. 8) that coincides with the trends of lineaments. The hydroxyl (clay?) bearing alteration NW of Lake Manyara is bounded with N-S faults. The same alteration exhibits an N-S trend NE of Meru volcano south of Oldoinyo-Lengai at the peak of Gelai volcano. Carbonates are seen at the peak of Oldoinyo-Lengai, defining an N-S orientation west of Lake Natron, attesting to them being structural controlled. Noteworthy is the presence of numerous hot springs within this area. Ferrous iron oxides exhibit preferential N-S and E-W orientation within the volcanic region which is not seen within the Precambrian metamorphic area. This suggests that the structures acted as "hydrothermal fluid pathways" that allowed fluid-rock interaction and eventual alteration of the host rocks. The iron oxide that dominates the volcanic region is probably a result of weathering of iron-bearing minerals from the mafic rocks.

The alteration zones observed during the fieldwork (Fig. 12) are located on WNW and ENE of the internal wall of the resurgent ash cone at the floor of Meru crater. They are characterized by acidic alteration in the form of grains of native sulphur observed during the fieldwork. This observation suggests that the structures trending NW- SE (west of Meru, Lembelos graben) extend beyond the Meru central crater and facilitate fluid flow well beyond its boundaries.

Based on the structural analysis, the orientation of volcanic centers and thermal manifestation in the study area we suggest that the N-S and NW - SE trending regional structures are responsible for the hydrothermal fluid flow and present potential target areas for further investigation for geothermal exploration.

In the Meru volcanic area, lake water samples (Aru-L2 and Aru-L3) largely deviated from WMWL (World Meteoric water line) and CARL (Continental Africa Rainwater Line) as well as having higher δD and δ ^{18}O values (Fig. 13).

The higher δD or δ ^{18}O values can result from evaporation or water-rock interaction at elevated temperature. Due to evaporation, the light hydrogen and oxygen isotopes are likely to be removed resulting in the abundance of the heavy hydrogen and oxygen isotopes. On the other hand, the higher δ ^{18}O values and large deviation from meteoric water lines can be caused by the water-rock interaction at elevated temperatures. During water-rock interaction, ^{16}O in spring water and ^{18}O in the rock are exchanged leading to the ratio of $\delta^{18}O$ being larger than the meteoric water lines (maybe need another source). Altogether, this suggests that the structures within these areas act as fluid pathways that are connected to the deep reservoir.

Hot and warm spring at Lake Natron emanates from fractures and colluviums at the base of the fault trending N-S. A carbon fluxes survey conducted by Lee et al. (2016) showed that CO_2 emanates from deep mantle sources, suggesting that the faults are conduits for fluid from the magmatic sources. These further support our inference that there is the existen-

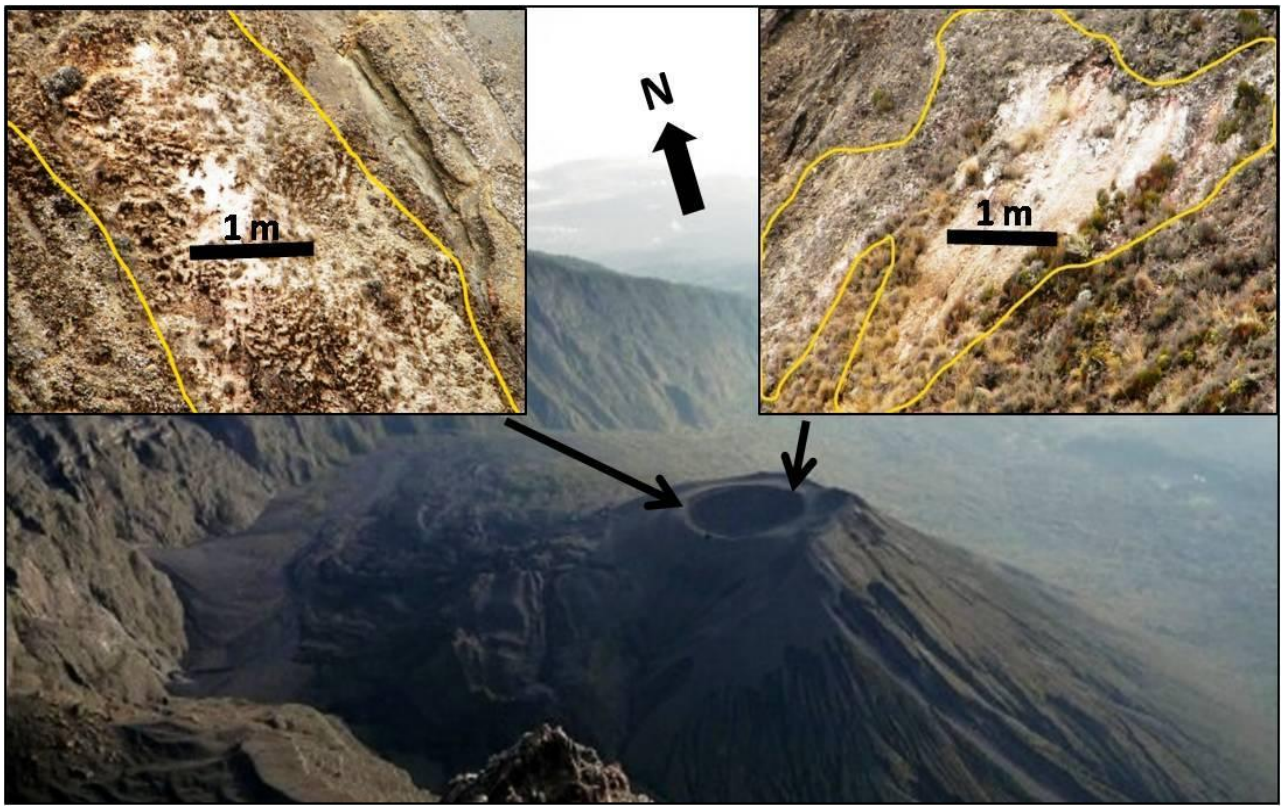

Fig. 12. Photos were taken during the fieldwork showing the alteration within the cone rim, which emerged on the floor of the Meru crater after the sector collapse

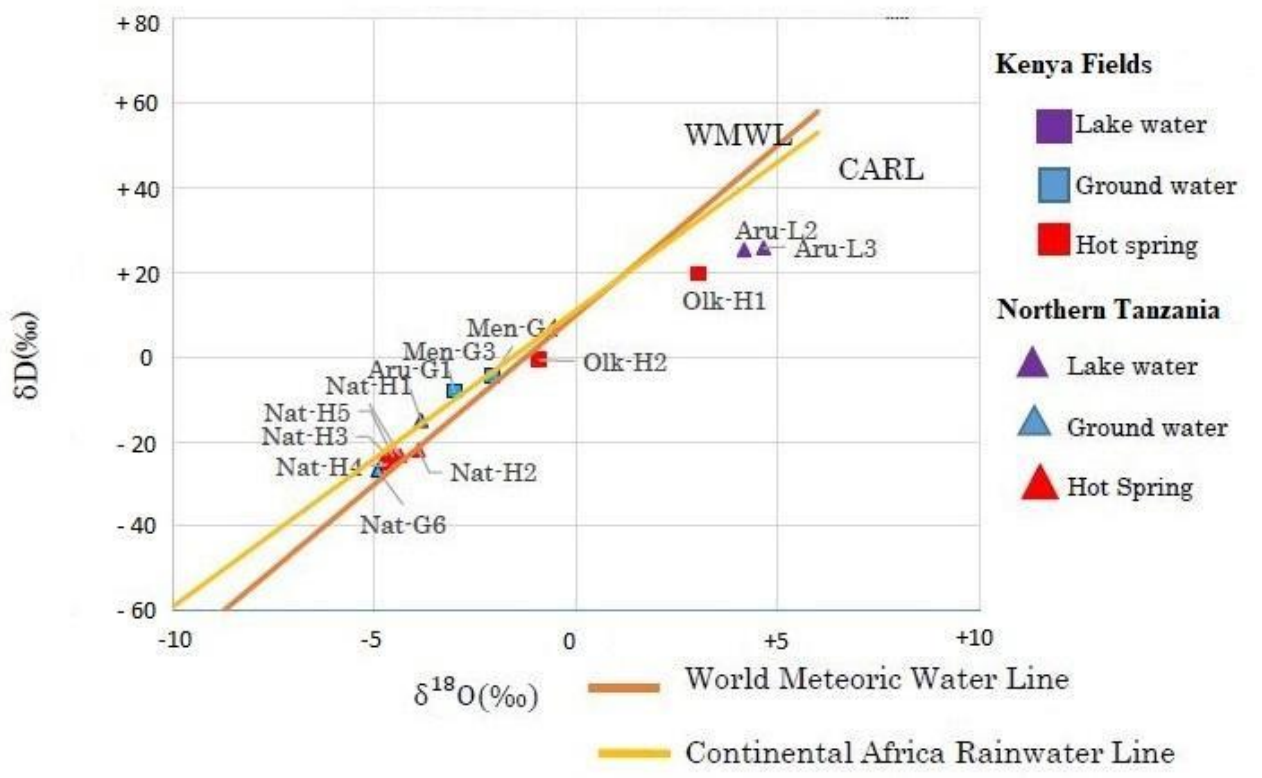

Fig. 13. Results of the hydrogen-oxygen stable isotopic composition of δD and $\delta^{18}O$.
(Nat- Lake Natron area, Aru – Meru Volcano area(Arusha National Park),
Olk –Olkaria geothermal field, Men- Menengai geothermal field

Table 2

Isotopic values of water collected during the fieldwork

Sample ID	$\delta^{18}O$	δD	Locality	Water type
Aru-G1	-3.85	-15.07	Meru	Ground water
Aru-L2	4.18	25.16	Meru	Lake water
Aru-L3	4.65	25.64	Meru	Lake water
Nat-H1	-4.37	-23.32	Natron area	Hot spring
Nat-H2	-3.92	-22.00	Natron area	Hot spring
Nat-H3	-4.71	-23.22	Natron area	Hot spring
Nat-H4	-4.69	-25.25	Natron area	Hot spring
Nat-H5	-4.53	-23.66	Natron area	Hot spring
Nat-G6	-4.92	-26.84	Natron area	Hot spring
Olk-H1	3.03	19.54	Olkaria	Thermal water
Olk-H2	-0.91	-0.63	Olkaria	Thermal water
Men-G3	-3.03	-8.26	Menengai	Ground water
Men-G4	-2.07	-4.58	Menengai	Ground water

ce of open faults that are permeable to allow the flow of hydrothermal fluid.

In the Natron area, almost all hot springs (Nat-H1, Nat-H2 ~Nat-H5) slightly deviate from meteoric water lines. This can be explained in terms of mixing meteoric water with magmatic fluid. These springs are controlled by the N-S structure along the shore of Lake Natron. The results from the analysis of one water sample (Olk-H1) from a geothermal well at Olkaria geothermal field, exhibit higher δD and $\delta^{18}O$ values that deviate from the meteoric water line toward higher $\delta^{18}O$ (Table 2). We suggest that these higher $\delta^{18}O$ values resulted from water-rock interaction at an elevated temperature at depth.

6. Conclusions

Understanding and evaluating the geological structure for the exploration of potential geothermal resources and other epithermal deposit is of principal importance. Open structures act as the conduits for hydrothermal fluids from their sources. These structures can be potential areas for drilling targets. The magmatism and tectonics of northern Tanzania make it a potentially substantial geothermal resource. The analysis of structures, on the basis of remote sensing and gravity data, suggests that, the areas affected by the N-S and NW–SE trending structures, present high potential for geothermal systems associated with tectono-volcanic activities during Pleistocene to recent.

References

1. *Abdelsalam, M., Stern, R.J., Berhane, W.G. (2000). Mapping gossans in arid environments with Landsat TM and SIR-C images: the Beddaho alteration zone in northern Eritrea. Journal of African Earth Sciences, 30 (4): 903–916. DOI: https://doi.org/10.1016/S0899-5362(00)00059-2*
2. *Albaric, J., Déverchére, J., Perrot, J., Jakovlev, A., Deschamps, A. (2010). Contrasted Seismogenic and Rheological Behaviours from Shallow and Deep Earthquake Sequences in the North Tanzanian Divergence, East Africa. Journal of African Earth Sciences, 58 (5): 799–811. DOI: https://doi.org/10.1016/j.jafrearsci.2009.09.005*
3. *Ali, A., Pour, A. (2014). Lithological Mapping and Hydrothermal Alteration Using Landsat 8 Data: A Case Study in Ariab Mining District, Red Sea Hills, Sudan. International Journal of Sciences: Basic and Applied Research, 3 (3): 199–208. DOI: https://doi.org/10.14419/ijbas.v3i3.2821*
4. *Baker, B.H., Mohr, P.A., Williams, L.A.J. (1972). Geology of the Eastern Rift System of Africa. Geological Society of America, (136) 67. DOI: https://doi.org/10.1130/SPE136*
5. *Bilim, F. (2007). Investigations into the tectonic lineaments and thermal structure of Kutahya-Denizli region, western Anatolia, from using aeromagnetic, gravity and seismological data. Physics of the Earth and Planetary Interiors, 165 (3–4): 135–146. DOI: https://doi.org/10.1016/j.pepi.2007.08.007*
6. *Björnsson, H. (2010), Understanding jökulhlaups: from tale to theory. Journal of Glaciology, 56 (200), 1002–1010. DOI: https://doi.org/10.3189/002214311796406086*
7. *Calvin, W.M., Littlefield, E.F., Kratt, C. (2015). Remote Sensing of Geothermal-Related Minerals for Resource Exploration in Nevada. Geothermics, 53: 517–526. DOI: https://doi.org/10.1016/j.geothermics.2014.09.002*
8. *Chavez, P.S., Sides, S.C., Anderson, J.A. (1991). Comparison of three different methods to merge multi-resolution and multi-spectral data: Landsat TM and SPOT panchromatic. Photogrammetric Engineering and Remote Sensing, 56: 459–467.*
9. *Dawson, J.B. (1992). Neogene Tectonics and Volcanicity in the North Tanzania sector of the Gregory Rift Valley: contrasts with the Kenya sector. Tectonophysics, 204 (1–2): 81–92. DOI: https://doi.org/10.1016/0040-*

1951(92)90271-7
10. Dawson, J.B. (2008). The Gregory Rift Valley and Neogene-Recent Volcanoes of Northern Tanzania. Geological Society of London, 33 (1–91).
11. Ebinger, C.J., Weinstein, A., Oliva, S.J., Roecker, S., Tiberi, C., Aman, M., Lambert, C., Witkin, E., Albaric, J., Gautier, S., Peyrat, S., Muirhead, J.D., Muzuka, A.N.N., Mulibo, G., Kianji, G., Wambura, R.F., Msabi, M., Rodzianko, A.R., Hadfield, R., Illsley-Kemp, F., Fischer, T.P. (2017). Fault-Magma Interactions during Early Continental Rifting: Seismicity of the Magadi-Natron-Manyara Basins. Geochemistry, Geophysics, Geosystems, 18 (10): 3662–3686. DOI: https://doi.org/10.1002/2017GC007027
12. Fairhead, J.D. (1976). The Structure of the Lithosphere beneath the Eastern Rift, East Africa, Deduced from Gravity Studies. Tectonophysics, 30 (3–4): 269–298. DOI: https://doi.org/10.1016/0040-1951(76)90190-6
13. Fairhead, J.D. (1980). The Structure of the Cross-Cutting Volcanic Chain of Northern Tanzania and Its Relation to the East African Rift System. Tectonophysics, 65 (3–4): 193–208. DOI: https://doi.org/10.1016/0040-1951(80)90074-8
14. Foster, A.N., Ebinger, C.J., Mbede, E., Rex, D. (1997). Tectonic development of the northern Tanzanian sector of the East African Rift System. Journal of Geological Society, London, 154: 689–700. DOI: https://doi.org/10.1144/gsjgs.154.4.0689
15. Franzson, H., Kristjansson, B.R., Gunnarsson, G., Björnsson, G., Hjartarson, A., Steingrimsson, B., Gunnlaugsson, E., Gislason, G. (2005). The Hengill-Hellisheiði Geothermal Field. Development of a Conceptual Geothermal Model. In Proceedings of the World Geothermal Congress, Antalya, Turkey. https://www.geothermal-energy.org/pdf/IGAstandard/WGC/2005/2632.pdf
16. Himematsu, Y., Furuya, M. (2015). Aseismic Strike-Slip Associated with the 2007 Dike Intrusion Episode in Tanzania. Tectonophysics, 656: 52–60. DOI: https://doi.org/10.1016/j.tecto.2015.06.005
17. Hutchison, W., Mather, T.A., Pyle, D.M., Biggs, J., Yirgu, G. (2015) Structural controls on fluid pathways in an active rift system: a case study of the Aluto volcanic complex. Geosphere, 11 (3): 542–562. DOI: https://doi.org/10.1130/GES01119.1
18. Le Gall, B., Nonnotte, P., Rolet, J., Benoit, M., Guillou, H., Mousseau-Nonnotte, M., Albaric, J., Deverchère, J. (2008). Rift Propagation at Craton Margin. Distribution of Faulting and Volcanism in the North Tanzanian Divergence (East Africa) during Neogene Times. Tectonophysics, 448 (1–4): 1–19. DOI: https://doi.org/10.1016/j.tecto.2007.11.005
19. Leat, P.T. (1991). Volcanological development of the Nakuru area of the Kenya rift valley. Journal of African Earth Sciences, 13 (3–4): 483–498. DOI: https://doi.org/10.1016/0899-5362(91)90111-B
20. Lee, H., Fischer, T.P., Muirhead, J.D., Ebinger, C.J., Kattenhorn, S.A., Sharp, Z.D., Kianji, G., Takahata, N., Sano, Y. (2016). Massive and Prolonged Deep Carbon Emissions Associated with Continental Rifting. Nature Geoscience, 9 (2): 145–149. DOI: https://www.nature.com/articles/ngeo2622#affil-auth
21. Loughlin, W.P. (1991). Principal Component Analysis for Alteration Mapping. Photogrammetric Engineering and Remote Sensing, 57 (9): 1163–1169. DOI: https://www.asprs.org/wpcontent/uploads/pers/1991journal/sep/1991_sep_1163-1169.pdf
22. Ma, Z.J., Gao, X.L., Song, Z.F. (2006). Analysis and tectonic interpretation to the horizontal gradient map calculated from Bouguer gravity data in the China mainland. Chinese Journal of Geophysics, 49 (1): 106–114. DOI: https://doi.org/10.1002/cjg2.816
23. Mana, S., Furman T., Turrin B.D., Feigenson M.D., Swisher, C.C. (2015). Magmatic Activity across the East African North Tanzanian Divergence Zone. Journal of the Geological Society, 172 (3): 368–389. DOI: https://doi.org/10.1144/jgs2014-07
24. Mia, M.B., Fujimitsu, Y. (2013). Landsat Thermal Infrared Based Monitoring of Heat Losses from Kuju Fumaroles Area in Japan. Procedia Earth and Planetary Science, 6: 114–120. DOI: https://doi.org/10.1016/j.proeps.2013.01.016
25. Mitchell, H.B. (2010). Image Fusion: Theories, Techniques and Applications, Springer: Berlin Heidelberg, 247 pp.
26. Mollel, G.F., Swisher, C.C., Feigenson, M.D., Carr, M.J. (2008). Geochemical Evolution of Ngorongoro Caldera, Northern Tanzania: Implications for Crust-Magma Interaction. Earth and Planetary Science Letters, 271 (1–4): 337–47. DOI: https://doi.org/10.1016/j.epsl.2008.04.014
27. Mshiu, E.E., Gläßer, C., Borg, G. (2015). Identification of hydrothermal paleofluid pathways, the pathfinders in the exploration of mineral deposits: A case study from the sukumaland greenstone belt, Lake Victoria Gold Field, Tanzania. Advances in Space Research, 55(4): 1117–1133. DOI: https://doi.org/10.1016/j.asr.2014.11.024
28. Nabighian, M.N. (1972). The Analytic Signal of Two-Dimensional Magnetic Bodies with Polygonal Cross-Section: Its Properties and Use for Automated Anomaly Interpretation. Geophysics, 37 (3): 507–517. DOI: https://doi.org/10.1190/1.1440276
29. Nabighian, M.N. (1974). Additional Comments on the Analytic Signal of Two-Dimensional Magnetic Bodies with Polygonal Cross-Section. Geophysics, 39 (1): 85–92. DOI: https://doi.org/10.1190/1.1440416
30. Nzaro, M.A. (1970). Geothermal Resources of Tanzania. Geothermics, 2 (2): 1039–1043. DOI: https://doi.org/10.1016/0375-6505(70)90412-8
31. Pilkington, M. (2007). Locating geologic contacts with magnitude transforms of magnetic data. Journal of Applied Geophysics, 63 (2): 80–89. DOI: https://doi.org/10.1016/j.jappgeo.2007.06.001
32. Phillips, J.D. (1997). Potential-Field Geophysical Software for the PC, version 2.2. USGS, Open-File Report 97-725. DOI: https://doi.org/10.3133/ofr97725
33. Phillips, J.D., Hansen, R.O., Blakely, R.J. (2007). The use of curvature in potential-field interpretation. Exploration Geophysics, 38 (2): 111–119. DOI: https://doi.org/10.1071/EG07014

34. Pour, A. B., Hashim, M., Genderen, J. (2013). Detection of Hydrothermal Alteration Zones in a Tropical Region Using Satellite Remote Sensing Data: Bau Goldfield, Sarawak, Malaysia. Ore Geology Reviews, 54: 181–196. DOI: https://doi.org/10.1016/j.oregeorev.2013.03.010
35. Rosenberg, M. (2017). Volcanic and Tectonic Perspectives on the Age and Evolution of the Wairakei-Tauhara Geothermal System. PhD Thesis, Victoria University of Wellington, New Zealand, 258–263. DOI: http://hdl.handle.net/10063/6436
36. Rymer, H., Brown, G.C. (1986). Gravity Fields and the Interpretation of Volcanic Structures: Geological Discrimination and Temporal Evolution. Journal of Volcanology and Geothermal Research, 27 (3–4): 229–254. DOI: https://doi.org/10.1016/0377-0273(86)90015-6
37. Saadi, N.M., Watanabe, K. (2008). Lineaments extraction and analysis in Eljufra area, Libya. Journal of Applied Remote Sensing, 2 (1), 023538. DOI: https://doi.org/10.1117/1.2994727
38. Sabins, F. (1997). Remote Sensing Principles and Interpretation, 3rd ed.; W.H. Freeman & Co: New York, 494 pp.
39. Sandwell, D.T., Smith W.H.F. (2009). Global marine gravity from retracked Geosat and ERS-1 altimetry: Ridge Segmentation versus spreading rate. Journal of Geophysical Research: Solid Earth, 114 (B1): B01411. DOI: https://doi.org/10.1029/2008JB006008
40. Sandwell, D.T., Garcia, E., Soofi, K., Wessel, P., Smith, W.H.F. (2013). Toward 1-mGal Accuracy in Global Marine Gravity from CryoSat-2, Envisat, and Jason-1. The Leading Edge, 32 (8): 892–899. DOI: https://topex.ucsd.edu/sandwell/publications/144.pdf
41. Sandwell, D.T., Müller, R.D., Smith, W.H.F., Garcia, E., Francis, R. (2014). New global marine gravity model from CryoSat-2 and Jason-1 reveals buried tectonic structure. Science, 346 (6205): 65–67. DOI: https://doi.org/10.1126/science.1258213
42. Simiyu, S.M., Keller, G.R. (1997). An Integrated Analysis of Lithospheric Structure across the East African Plateau Based on Gravity Anomalies and Recent Seismic Studies. Tectonophysics, 278 (1–4): 291–313. DOI: https://doi.org/10.1016/S0040-1951(97)00109-1
43. Ulusoy, İ. (2016). Temporal Radiative Heat Flux Estimation and Alteration Mapping of Tendürek Volcano (Eastern Turkey) Using ASTER Imagery. Journal of Volcanology and Geothermal Research, 327: 40–54. DOI: https://doi.org/10.1016/j.jvolgeores.2016.06.027
44. Wilkinson, P., Mitchell, J.G., Cattermole, P.J., Downie, C. (1986). Volcanic Chronology of the Men-Kilimanjaro Region, Northern Tanzania. Journal of the Geological Society, 143 (4): 601–605. DOI: https://doi.org/10.1144/gsjgs.143.4.0601

Authors Contribution: All authors have contributed equally to this work

Оцінка геологічних структур і геотермальних ресурсів у вулканічній зоні Північної Танзанії за допомогою дистанційного зондування та аналізу даних гравітації

Альбано Махеча [1, 3]
кафедра корпоративних програм ресурсного інжинірингу,
інженерний факультет, [1] Університет Кюсю, Фукуока, Японія;
[3] Танзанія Геотермал Девелопмент Компані Лімітед, Дар-ес-Салам, Танзанія;
Нуреддін Сааді [2]
кафедра геологічної інженерії, інженерний факультет,
[2] Університет Тріполі, Університетська дорога, Тріполі, Лівія;
Ессам Абауд [4, 5]
Центр дослідження геонебезпек,
[4] Університет короля Абдулазіза, Джидда, Саудівська Аравія;
[5] Національний науково-дослідний інститут астрономії та геофізики, Каїр, Єгипет;
Акіра Імаї [1]
кафедра інженерії ресурсів Землі, інженерний факультет;
Котаро Йонезу [1]
кафедра інженерії ресурсів Землі, інженерний факультет

Вулканічна місцевість Північної Танзанії була предметом оцінки геотермального потенціалу протягом останніх чотирьох десятиліть. Регіон характеризується вулканічною та тектонічною активністю від неогену до сучасності. Це попереднє дослідження, засноване на даних дистанційного зондування, хімії води, даних гравітації, геологічних структурах і розподілі вулканічних центрів, повідомляє про виявлені геотермальні прояви та обговорює наслідки для шляхів геотермальних рідин. Киснево-водневі ізотопні дані з проб води вказують на те, що вони були залучені до гідротермальної системи. Район розбіжності Північної Танзанії (NTD), що характеризується вулканічною та тектонічною діяльністю від неогену до сучасності. Останні вулканічні та тектонічні дії включають

виверження попелового конуса та лавового купола на дні кратера Меру століття тому, вторгнення дайк та виверження вулкана на південь від вулкана Гелай та вулкана Олдойньо-Ленгай відповідно. Фумарольна діяльність і гарячі джерела домінують у відносно молодому вулканічному районі на північному сході та в північній частині NTD. Місія Shuttle Radar Topography Mission (SRTM), зображення Landsat 8 Operational Land Imager (OLI), аналіз ізотопів води та гравітаційні дані були використані для вилучення та аналізу поверхневих і підповерхневих геологічних ліній і картування зон гідротермальних змін у досліджуваній області. Гідротермальна зміна використовується для оцінки та ідентифікації проникних структур. Аналіз та інтерпретація довжини та трендів вилучених лінеаментів були використані для дослідження тектонічної еволюції. Геологічна карта досліджуваної території була оцифрована з існуючих геологічних карт і віку гірських порід, щоб окреслити вулканічну активність і пов'язані з нею лінеаменти на основі віку літологічного домену. Більш високі значення $\delta^{18}O$ та велике відхилення від ліній метеоритної води припускають, що це пов’язано з взаємодією флюїдів із вміщуючими породами при підвищених температурах. Вони відповідають відкритим структурам, які діють як канали для потоку рідини. Дані потенційної сили тяжіння показують басейноподібну структуру, що тягнеться в напрямку Пн-Пн-З. Гравітаційні дані показують, що блоки фундаменту поступово поглиблюються до центральної частини і що вони контролюються двома основними системами розломів, спрямованих відповідно на Пн-Пд та Пн-З-Пд. Гравітаційні дані, представлені тут, надають нові обмеження щодо тектонічної еволюції та геотермальних ресурсів досліджуваної території.

***Ключові слова**: дистанційне зондування, гравітація, геотермальний, Танзанія, структури, ізотоп.*

Внесок авторів: всі автори зробили рівний внесок у цю роботу

Надійшла 25 вересня 2023 р.
Прийнята 27 жовтня 2023 р.